



Full $\mathcal{O}(\alpha)$ electroweak radiative corrections to $e^+e^- \rightarrow e^+e^-\gamma$ at the ILC with GRACE-Loop



P.H. Khiem^{a,b}, Y. Kurihara^a, J. Fujimoto^a, T. Ishikawa^a, T. Kaneko^a, K. Kato^c,
N. Nakazawa^c, Y. Shimizu^a, T. Ueda^d, J.A.M. Vermaseren^e, Y. Yasui^f

^a KEK, Oho 1-1, Tsukuba, Ibaraki 305-0801, Japan

^b SOKENDAI University, Shonan Village, Hayama, Kanagawa 240-0193, Japan

^c Kogakuin University, Shinjuku, Tokyo 163-8677, Japan

^d Karlsruhe Institute of Technology (KIT), D-76128 Karlsruhe, Germany

^e Nikhef, Science Park 105, 1098 XG Amsterdam, the Netherlands

^f Tokyo Management College, Ichikawa, Chiba 272-0001, Japan

ARTICLE INFO

Article history:

Received 1 September 2014

Received in revised form 14 November 2014

Accepted 25 November 2014

Available online 2 December 2014

Editor: G.F. Giudice

ABSTRACT

By using the GRACE-Loop system, we calculate the full $\mathcal{O}(\alpha)$ electroweak radiative corrections to the process $e^+e^- \rightarrow e^+e^-\gamma$, which is important for future investigations at the International Linear Collider (ILC). With the GRACE-Loop system, the calculations are checked numerically by three consistency tests: ultraviolet finiteness, infrared finiteness, and gauge-parameter independence. The results show good numerical stability when quadruple precision is used. In the phenomenological results, we find that the electroweak corrections to the total cross section range from $\sim -4\%$ to $\sim -21\%$ when \sqrt{s} varies from 250 GeV to 1 TeV. The corrections also significantly affect the differential cross sections, which are a function of energies and angles of the final state particles. Such corrections will play an important role in the high-precision program at the ILC.

© 2014 The Authors. Published by Elsevier B.V. This is an open access article under the CC BY license (<http://creativecommons.org/licenses/by/3.0/>). Funded by SCOAP³.

1. Introduction

The goals of the International Linear Collider (ILC) are not only to precisely measure the properties of the Higgs particle, the top quark, and vector boson interactions but also to search for physics beyond the Standard Model. The high-precision measurements are expected to have a typical statistical error of less than 0.1%. This requires a very precise determination of the luminosity.

At the ILC, the integrated luminosity is measured [1] by counting Bhabha events and comparing the result with the corresponding theoretical cross section:

$$\int dt \mathcal{L} = \frac{N_{\text{events}} - N_{\text{bgk}}}{\epsilon \cdot \sigma_{\text{theory}}}. \quad (1)$$

In this formula, N_{events} (N_{bgk}) is the number of the observed Bhabha events (the estimated background events); σ_{theory} is the Bhabha scattering cross section, which is calculated by using the

perturbation theory; ϵ is the total selection efficiency for the events and $\int dt \mathcal{L}$ is the integrated luminosity.

A precise calculation of Bhabha scattering is important for a high-luminosity measurement, because the determination of all other cross sections depend on it. Thus, the one-loop electroweak corrections to Bhabha scattering are of considerable interest to many researchers. The full one-loop electroweak corrections to the $e^+e^- \rightarrow e^+e^-$ reaction were calculated many years ago in Refs. [2–5] and confirmed independently in Refs. [6,7]. The corrections contribute significantly to the total cross section; about $\mathcal{O}(10\%)$ at high energy.

It is clear that the high-precision program at the ILC must consider the two-loop electroweak corrections to Bhabha scattering; many researchers have worked at these calculations for many years. However, the calculations were mostly performed at the level of two-loop QED corrections. To date, full two-loop electroweak corrections are not available. We refer here to several typical papers for two-loop QED calculations. A two-loop photonic correction to this process was calculated in Refs. [8,9]. In addition, two-loop QED corrections that maintain the electron mass in the squared amplitude are presented in Ref. [10]. In a later publication,

E-mail address: khiemph@post.kek.jp (P.H. Khiem).

the same group included the soft-photon-emission contribution to the differential cross section, as presented in Ref. [11]. We also want to mention the calculation of two-loop QED corrections to the Bhabha process which involves vacuum polarization by heavy fermions of arbitrary mass in Refs. [12,13], two-loop QED corrections related to virtual hadronic and leptonic contributions to Bhabha scattering also performed in Refs. [14,15]. An approximation of the two-loop electroweak corrections to Bhabha scattering was computed in Ref. [17]. In this calculation, the authors considered the dominant logarithmically enhanced two-loop electroweak corrections to the differential cross section in the high-energy limit and at large scattering angles. Moreover, a two-loop weak corrections contributed from a heavy top quark to Bhabha scattering were found in Ref. [18].

The perspectives of the present calculation are as follows: To correct the number of Bhabha events, a precise evaluation of its background is required. Experiments may misidentify $e^+e^- \gamma$ as e^+e^- events because (i) the photon is a hard bremsstrahlung photon that can escape the detector, (ii) the photon is a soft bremsstrahlung photon that has a small opening angle with respect to the final electron (or positron), or (iii) the photon is emitted in parallel to the beam axis. With these misidentifications, the process $e^+e^- \rightarrow e^+e^- \gamma$ is one channel that contributes significantly to the background of Bhabha events. Hence the precise calculation of the process is of great importance. Furthermore, in the framework of calculating the full two-loop corrections to Bhabha scattering, one-loop electroweak corrections to $e^+e^- \rightarrow e^+e^- \gamma$ with a soft bremsstrahlung photon are necessary; they should cancel against the infrared divergences which appear at the level of two-loop corrections to Bhabha scattering. Last but by no means least, the process will be a good candidate for luminosity measurements at the ILC, provided these theoretical calculations are well under control.

We refer to a few additional papers that should be mentioned. The lowest-order calculation of the soft-bremsstrahlung process is reported in Ref. [19]. Moreover, the one-loop QED corrections to the hard-bremsstrahlung process $e^+e^- \rightarrow e^+e^- \gamma$ is available in Ref. [16]. An analytical calculation of one-loop QED corrections to the process $e^+e^- \rightarrow e^+e^- \gamma$ is also calculated in Ref. [20].

To achieve our eventual target, the calculation of two-loop corrections to Bhabha scattering, several steps are involved, the first of which is to consider the process as a candidate for luminosity measurements at the ILC, because it provides a useful framework for our final objective. This is what we present in this paper. In particular, we focus on studying the impact of electroweak corrections to the total cross section and to the relevant distributions such as the cross sections that are a functions of energies, and angles of the final state particles. We will incorporate the soft photon bremsstrahlung and subsequently the two-loop corrections to Bhabha scattering in future publications.

The layout of the paper is as follows: In Section 2, we present a short introduction to the GRACE-Loop system and the numerical tests of the calculation. In Section 3, we present the phenomenological results of the calculation. Conclusions and plans for future work are presented in Section 4.

2. GRACE Loop and the $e^+e^- \rightarrow e^+e^- \gamma$ process

2.1. GRACE Loop

GRACE Loop is a generic program that automates the calculation of high-energy physics processes at the one-loop level. The program is described in detail in Ref. [21], where a variety of electroweak processes with two particles in the final state are

presented and compared with other papers. The GRACE-Loop system was also used to calculate processes with three particles in the final state, such as $e^+e^- \rightarrow ZHH$ [22], $e^+e^- \rightarrow t\bar{t}H$ [23], and $e^+e^- \rightarrow \nu\bar{\nu}H$ [24]. These calculations were performed independently by several groups; for example, the processes $e^+e^- \rightarrow ZHH$ [25], $e^+e^- \rightarrow t\bar{t}H$ [26–28], and $e^+e^- \rightarrow \nu\bar{\nu}H$ [29,30]. In addition, the $e^+e^- \rightarrow \nu_\mu\bar{\nu}_\mu HH$ [31] reaction was calculated by using the GRACE-Loop system.

In the GRACE-Loop system, the renormalization is performed with the on-shell renormalization condition of the Kyoto scheme, as described in Ref. [32]. Ultraviolet (UV) divergences are regulated by dimensional regularization, and infrared (IR) divergences are regularized by giving the photon an infinitesimal mass λ . In the current version there are no soft external gluons.

The GRACE-Loop system uses the symbolic-manipulation package FORM [33,34] to handle all Dirac and tensor algebra in n dimensions. It symbolically reduces all tensor one-loop integrals to scalar integrals. Eventually, the amplitude of the given processes will be written in terms of FORTRAN subroutines on a diagram-by-diagram basis.

Ref. [21] describes the method used by the GRACE-Loop system to reduce tensor one-loop five- and six-point functions to one-loop four-point functions. The tensor one-, two-, three-, and four-point functions are then reduced to scalar one-loop integrals that are numerically evaluated by one of the FF [35] or LoopTools [36] packages.

The GRACE-Loop program uses so-called nonlinear gauge fixing terms [37] in the Lagrangian, which are defined as

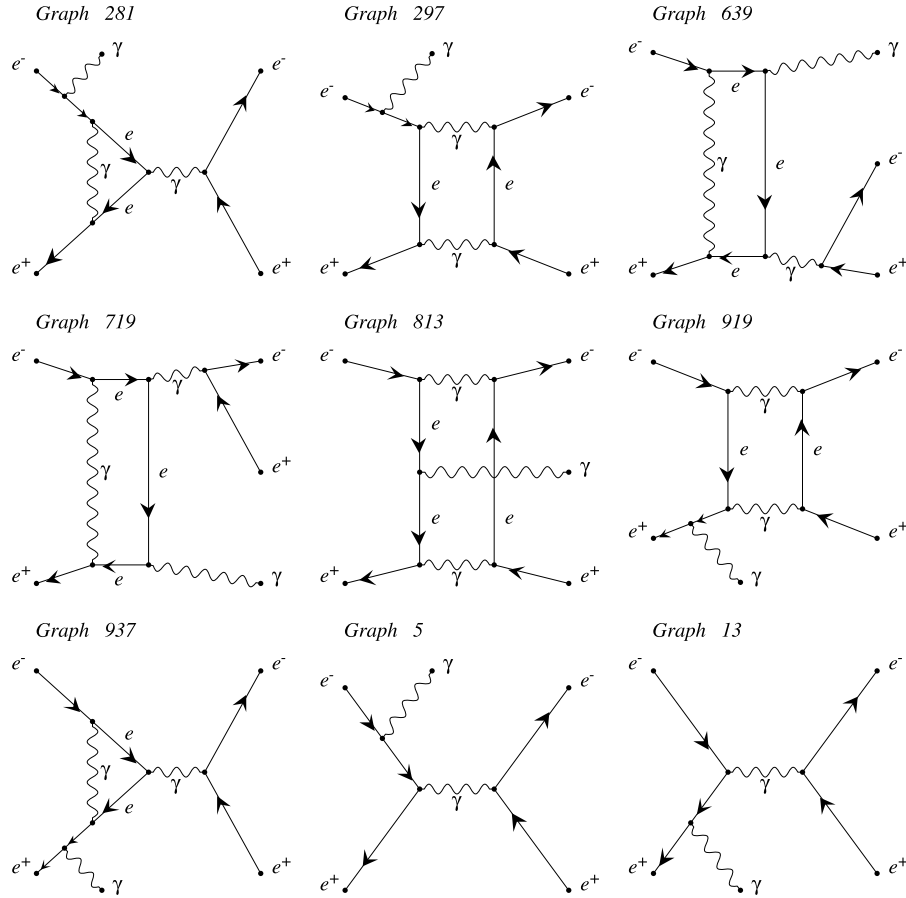
$$\begin{aligned} \mathcal{L}_{GF} = & -\frac{1}{\xi_W} |(\partial_\mu - ie\tilde{\alpha}A_\mu - ig_{CW}\tilde{\beta}Z_\mu)W^{\mu+}|^2 \\ & + \xi_W \frac{g}{2} (v + \tilde{\delta}H + i\tilde{\kappa}\chi_3)\chi^+|^2 \\ & - \frac{1}{2\xi_Z} \left(\partial \cdot Z + \xi_Z \frac{g}{2C_W} (v + \tilde{\epsilon}H)\chi_3 \right)^2 - \frac{1}{2\xi_A} (\partial \cdot A)^2. \end{aligned} \quad (2)$$

We are working in the R_ξ -type gauges with the condition $\xi_W = \xi_Z = \xi_A = 1$ (also called the 't Hooft–Feynman gauge) in which there is no longitudinal contribution to the gauge propagator. This choice not only has the advantage of making the expressions much simpler but also avoids unnecessarily large cancellations, high tensor ranks in one-loop integrals, and extra powers of momenta in the denominators, which cannot be handled by the FF and LoopTools packages. The implementation of nonlinear gauge-fixing terms provides a powerful tool to check the results in a consistent way. After all, the results must be independent of the nonlinear gauge parameters, as will be discussed in greater detail in Section 2.2.

In its latest version, the GRACE Loop system can use the axial gauge in the projection operator for external photons. This resolves a problem with large numerical cancellations, which is very useful when calculating processes at small angle and energy cuts for the final-state particles. Moreover, it provides a useful tool to check the consistency of the results, which due to the Ward identities, are independent of the choice of the gauge. This method was applied to the process $e^+e^- \rightarrow t\bar{t}\gamma$ in Ref. [38], and we apply it here as well. For the integration steps, we use a parallel version of BASES [40] with a message-passing interface [41] to reduce the calculation time.

2.2. The $e^+e^- \rightarrow e^+e^- \gamma$ process

The full set of Feynman diagrams with the nonlinear gauge fixing, as described in the previous section, consists of 32 tree diagrams and 3456 one-loop diagrams. This includes the counterterm



produced by GRACEFIG

Fig. 1. Typical Feynman diagrams for the reaction $e^+e^- \rightarrow e^+e^-\gamma$ as generated by the GRACE-Loop system.

diagrams. In Fig. 1, we show some selected diagrams. For this calculation, we apply an axial gauge for the external photon by using the polarization sum of the photons as follows:

$$\mathcal{P}(\lambda) = \sum_{\lambda=0}^3 \epsilon_{\lambda}^{\mu}(p) \epsilon_{\lambda}^{\nu}(p) \rightarrow -g^{\mu\nu} + \frac{n^{\mu} p^{\nu} + n^{\nu} p^{\mu}}{n \cdot p} - n^2 \frac{p^{\mu} p^{\nu}}{(n \cdot p)^2}, \quad (3)$$

where p^{μ} and ϵ_{λ}^{μ} correspond to the 4-momentum and the polarization vector of the external photon respectively. The axial vector n takes the form

$$n = (p^0, -\vec{p}). \quad (4)$$

With this choice, the third term in Eq. (3) vanishes, which means that we are working in the light-cone gauge for the photon. The advantage of using the axial gauge for the external photon is that the worst numerical cancellations between the diagrams are avoided.

Before running the Monte Carlo integration for the process, the calculation is checked numerically by three consistency tests. These are UV and IR finiteness and gauge-parameter independence. The general idea of these tests is now described.

The full $\mathcal{O}(\alpha)$ electroweak cross section considers the tree graphs and the full one-loop virtual corrections as well as the soft and hard bremsstrahlung contributions. In general, the total cross section in full one-loop electroweak radiative corrections is given by

$$\begin{aligned} \sigma_{\mathcal{O}(\alpha)}^{e^-e^+\gamma_H} &= \int d\sigma_{\mathbf{T}}^{e^-e^+\gamma_H} + \int d\sigma_{\mathbf{V}}^{e^-e^+\gamma_H}(C_{UV}, \{\tilde{\alpha}, \tilde{\beta}, \tilde{\delta}, \tilde{\epsilon}, \tilde{\kappa}\}, \lambda) \\ &+ \int d\sigma_{\mathbf{T}}^{e^-e^+\gamma_H} \delta_{\text{soft}}(\lambda \leq E_{\gamma_S} < k_c) \\ &+ \int d\sigma_{\mathbf{H}}^{e^-e^+\gamma_H \gamma_S}(E_{\gamma_S} \geq k_c). \end{aligned} \quad (5)$$

In this formula, $\sigma_{\mathbf{T}}^{e^-e^+\gamma_H}$ is the tree-level cross section, $\sigma_{\mathbf{V}}^{e^-e^+\gamma_H}$ is the cross section due to the interference between the one-loop (including counterterms) and the tree diagrams. The contribution must be independent of the UV-cutoff parameter (C_{UV}) and the nonlinear gauge parameters ($\tilde{\alpha}, \tilde{\beta}, \tilde{\delta}, \tilde{\epsilon}, \tilde{\kappa}$). Because of the way we regularize the IR divergences, $\sigma_{\mathbf{V}}^{e^-e^+\gamma_H}$ depends on the photon mass λ . This λ dependence must cancel against the soft-photon contribution, which is the third term in Eq. (5). The soft-photon contribution can be factorized into a soft factor, which is calculated explicitly in Ref. [39], and the cross section from the tree diagrams.

In Tables 2, 4, and 3 in Appendix A, we present the numerical results for the checks of UV finiteness, gauge invariance, and the IR finiteness for one random point in phase space, calculated with quadruple precision. The results are stable over a range of 20 digits. The different precisions are due to the ways in which these parameters occur in the formulas: C_{UV} occurs only linearly as an extra term, and the nonlinear gauge parameters occur as products in terms that are by themselves typically much larger than the remaining terms. The IR regulator λ contributes mainly because of

its appearance in the denominators and hence occurs inside logarithms. Consequently, the C_{UV} checks show an agreement in more digits than the other checks.

Finally, we consider the contribution of the hard photon bremsstrahlung, $\sigma_{\mathbf{H}}^{e^-e^+\gamma_H\gamma_S}(k_c)$. This part is the process $e^+e^- \rightarrow e^-e^+\gamma_H\gamma_S$ with an added hard bremsstrahlung photon. The process is generated by the tree-level version of the GRACE system [42] with the phase space integration performed by BASES. By adding this contribution to the total cross section, the final results must be independent of the soft-photon cutoff energy k_c . Table 5 in Appendix A shows the numerical result of the check of k_c stability. By changing k_c from 10^{-3} GeV to 0.1 GeV, the results are consistent to an accuracy better than 0.04% (this accuracy is better than that in each Monte Carlo integration). For the check of k_c stability, note that we have two photons at the final state. One photon is the hard photon to which we apply an energy cut of $E_{\gamma_H}^{\text{cut}} \geq 10$ GeV and an angle cut of $10^\circ \leq \theta_{\gamma_H}^{\text{cut}} \leq 170^\circ$. The second photon is the soft photon whose energy is greater than k_c and smaller than the energy of the first photon.

Having verified the stability of the results, we proceed to compute the physics of the process. Hereafter, we use $\lambda = 10^{-21}$ GeV, $C_{UV} = 0$, $k_c = 10^{-3}$ GeV, and $\tilde{\alpha} = \tilde{\beta} = \tilde{\delta} = \tilde{\kappa} = \tilde{\varepsilon} = 0$. To reduce the calculation time, we neglect the diagrams that contain the coupling of the Higgs boson to the electron and positron in the integration step because its contribution is less than the statistical error of the Monte Carlo integration.

3. Results of the calculation

We used the following input parameters for the calculation: The fine structure constant in the Thomson limit is $\alpha^{-1} = 137.0359895$.

The mass of the Z boson is $M_Z = 91.1876$ GeV and its decay width is $\Gamma_Z = 2.35$ GeV.

The mass of the Higgs boson is taken to be $M_H = 126$ GeV.

In the on-shell renormalization scheme we like to take the mass of the W boson as an input parameter. Because of the limited accuracy of the measured value, we take the value that is derived from the electroweak radiative corrections to the muon decay width (Δr) [43] with $G_\mu = 1.16639 \times 10^{-5}$ GeV⁻². Therefore, M_W is a function of M_H . This results in $M_W = 80.370$ GeV as explained in Section 3.1, corresponding to $\Delta r = 2.49\%$.

For the lepton masses we take $m_e = 0.51099891$ MeV, $m_\mu = 105.658367$ MeV and $m_\tau = 1776.82$ MeV.

For the quark masses, we take $m_u = 63$ MeV, $m_d = 63$ MeV, $m_c = 1.5$ GeV, $m_s = 94$ MeV, $m_t = 173.5$ GeV, and $m_b = 4.7$ GeV.

Because the process considered in this paper is a candidate for luminosity measurements, the full $\mathcal{O}(\alpha)$ electroweak corrections to $e^-e^+ \rightarrow e^-e^+\gamma$ are evaluated by applying cuts that are suitable for this purpose. For the final-state particles, we apply an energy cut $E^{\text{cut}} \geq 10$ GeV and an angle cut $10^\circ \leq \theta^{\text{cut}} \leq 170^\circ$ with respect to the beam axis. Moreover, to isolate the photon from the electron (or positron), we apply an opening angle cut between the photon and the e^- (e^+) of 10° . Finally, to distinguish $e^-e^+\gamma$ events from $\gamma\gamma$ events, we apply an angle cut of 10° between the electron and the positron in the final state. The results for this case are presented in the following subsection.

3.1. Total cross section and electroweak corrections

The total cross section is calculated by using Eq. (5). The relative correction is then defined in the α scheme as

$$\delta_{EW} = K_{EW} - 1 \quad (6)$$

Table 1

The total cross section and the electroweak corrections as a function of the center-of-mass energy.

\sqrt{s} [GeV]	$\sigma_{\mathbf{T}}$ [pb]	$\sigma_{\mathcal{O}(\alpha)}^{\text{QED}}$ [pb]	$\sigma_{\mathcal{O}(\alpha)}$ [pb]	δ_{QED} [%]	δ_{EW} [%]	δ_{W} [%]	$\delta_{\text{W}}^{G_\mu}$ [%]
250	9.746	9.269	9.317	-4.89	-4.40	0.49	-4.49
350	5.684	5.244	5.254	-7.74	-7.57	0.17	-4.81
500	3.175	2.839	2.811	-10.58	-11.47	-0.89	-5.87
700	1.817	1.564	1.534	-13.92	-15.58	-1.66	-6.64
1000	1.001	0.828	0.789	-17.28	-21.18	-3.90	-8.88

$$= \frac{\sigma_{\mathcal{O}(\alpha)}}{\sigma_{\text{tree}}} - 1, \quad (7)$$

where the term K_{EW} is the ratio of the full cross section up to one-loop radiative corrections to the cross section from tree-level contributions.

In the GRACE-Loop system, the QED corrections can be calculated separately by selecting individual QED diagrams and their counterterms. As expressed in the following equation, the total QED cross section is then normalized to the cross section of the full tree diagrams to extract the QED corrections:

$$\delta_{\text{QED}} = \frac{\sigma_{\mathbf{V+S+H}}^{\text{QED}}}{\sigma_{\text{tree}}}. \quad (8)$$

The next equation gives the genuine weak correction in the α scheme:

$$\delta_{\text{W}} = \delta_{\text{EW}} - \delta_{\text{QED}}. \quad (9)$$

Having subtracted the genuine weak corrections in the α scheme, one can express the correction in the G_μ scheme. This approach is also called the improved Born approximation, where the fine structure constant runs from the Thomson-limit condition to the M_Z^2 scale. Some of the high-order corrections are related to two-point functions, which are connected to light fermions and absorbed into the tree-level calculation. To obtain the corrections in this scheme, we subtract the universal weak correction obtained from Δr as follows¹:

$$\delta_{\text{W}}^{G_\mu} = \delta_{\text{W}} - 2\Delta r, \quad (10)$$

with $\Delta r = 2.49\%$ for $M_H = 126$ GeV.

Table 1 shows the total cross section and the electroweak corrections as a function of \sqrt{s} . The center-of-mass energy ranges from 250 GeV (which is near the threshold of $M_H + M_Z$) to 1 TeV.

We find that the electroweak (QED) corrections in the α scheme vary from $\sim -4\%$ ($\sim -5\%$) to $\sim -21\%$ ($\sim -17\%$) as \sqrt{s} varies from 250 GeV to 1 TeV. The results given in Table 1 show clearly that the QED corrections make the dominant contribution compared with the weak corrections. The weak corrections in the G_μ scheme vary from $\sim -4\%$ to $\sim -9\%$ as \sqrt{s} varies from 250 GeV to 1 TeV. The weak corrections in the high-energy region are attributed to the enhancement contribution of the single Sudakov logarithm. Its contribution can be estimated as follows:

$$\delta_{\text{W}}^{G_\mu} \sim -\frac{\alpha(M_Z^2)}{\pi \sin^2 \theta_W} \log\left(\frac{s}{M_Z^2}\right) \sim \mathcal{O}(-10\%) \quad \text{at } \sqrt{s} = 1 \text{ TeV}. \quad (11)$$

It is clear that the corrections make a sizable contribution to the total cross section and cannot be ignored for the high-precision program at the ILC.

¹ The order of α , which comes from the coupling of real photons to fermions, must be calculated under the conditions of the Thomson limit. The order α^2 runs from the Thomson limit to the M_Z^2 scale. Overall, these considerations lead to the factor 2 in Eq. (10).

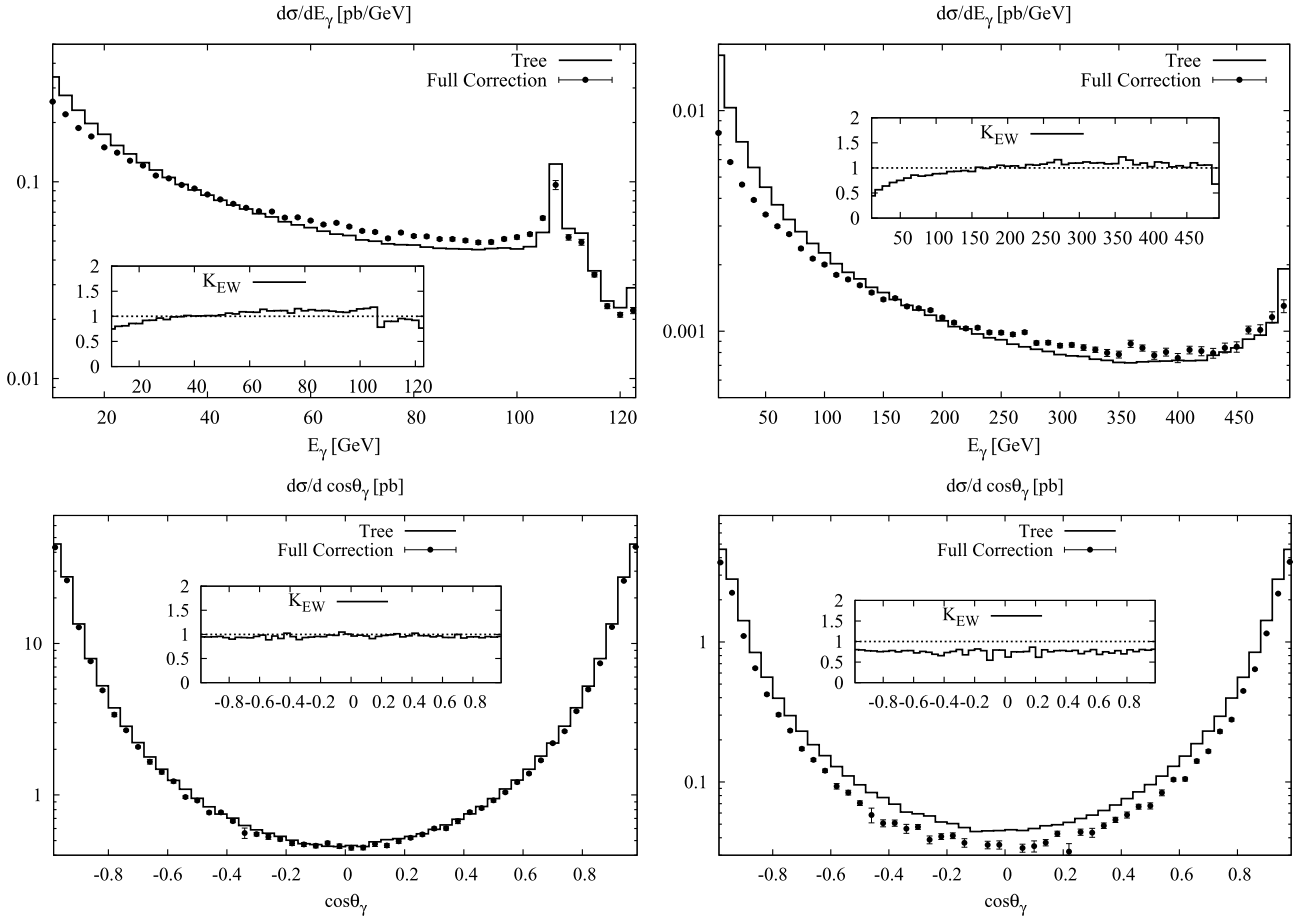


Fig. 2. Differential cross sections as a function of photon energy and $\cos\theta_\gamma$ at (left panel) $\sqrt{s} = 250$ GeV and (right panel) $\sqrt{s} = 1$ TeV.

3.2. Relevant distributions

We now generate the relevant distributions such as the cross sections, which are a function of energies, and angles of the final state particles. In these distributions, the solid lines represent the tree-level calculation, and the points with error bars include the full radiative corrections. The left (right) figures show the given distributions at $\sqrt{s} = 250$ GeV (1 TeV). The term K_{EW} is also shown with these distributions to estimate the electroweak corrections to the differential cross sections. Fig. 2 presents the cross-section distributions as a function of the photon energy for $\sqrt{s} = 250$ GeV and $\sqrt{s} = 1$ TeV. Overall, the cross section decreases with increasing photon energy. At $\sqrt{s} = 250$ GeV, two peaks appear, one at $E_\gamma = \frac{s - M_Z^2}{2\sqrt{s}}$ and one at $\frac{\sqrt{s}}{2}$. The first peak corresponds to the photon energy recoiling against an on-shell Z boson, and the right peak corresponds to the photon energy recoiling against a virtual photon that creates a small-mass electron-positron pair. Due to the high energy the peaks overlap within our resolution at $\sqrt{s} = 1$ TeV. The distributions also clearly show that the radiative corrections make a sizeable impact and are important for the luminosity monitor at the ILC. The lower part of Fig. 2 shows the angular distributions of the photon at $\sqrt{s} = 250$ GeV and $\sqrt{s} = 1$ TeV. The cross section is symmetric with respect to $\cos\theta_\gamma$. The radiative corrections make a more significant contribution at $\sqrt{s} = 1$ TeV compared with their contribution at 250 GeV center-of-mass energy.

Fig. 3 presents the differential cross sections as a function of the positron energy for $\sqrt{s} = 250$ GeV and $\sqrt{s} = 1$ TeV. The cross section increases with increasing positron energy. Two peaks appear

in the distributions; the first of which is attributed to the highest-energy positron $E_{e^+} \sim \frac{\sqrt{s}}{2}$ (or the smallest invariant mass of the photon and electron). The second peak corresponds to a minimum-energy photon emitted from the electron. This peak appears at $E_{e^+} \sim \frac{\sqrt{s}}{2} - E_\gamma^{\min}$. Within our resolution at $\sqrt{s} = 1$ TeV, the two peaks overlap. The positron angular distributions in the final state are shown at $\sqrt{s} = 250$ GeV and $\sqrt{s} = 1$ TeV in the lower part of Fig. 3. Again, the radiative corrections make a sizeable impact.

4. Conclusions

Using the GRACE-Loop system, we calculated the full $\mathcal{O}(\alpha)$ electroweak radiative corrections to the $e^+e^- \rightarrow e^+e^-\gamma$ process for energies to be expected at the International Linear Collider.

The GRACE-Loop system incorporates a generalized nonlinear gauge-fixing condition that includes five gauge parameters. Combined with UV, IR finiteness and cutoff stability tests, they provide a powerful tool for testing the consistency of the results. The tests indicate that the numerical results are stable when quadruple precision is used.

We show that the full electroweak radiative corrections vary from $\sim -4\%$ to $\sim -21\%$ for a center-of-mass energy ranging from 250 GeV to 1 TeV. These corrections have a sizeable impact on the differential cross sections. Therefore, this calculation is important for determining the luminosity at the ILC.

In future work, we plan to incorporate the process with a soft bremsstrahlung photon and to consider the calculation for full two-loop corrections to Bhabha scattering when the system for two-loop functions library is available.

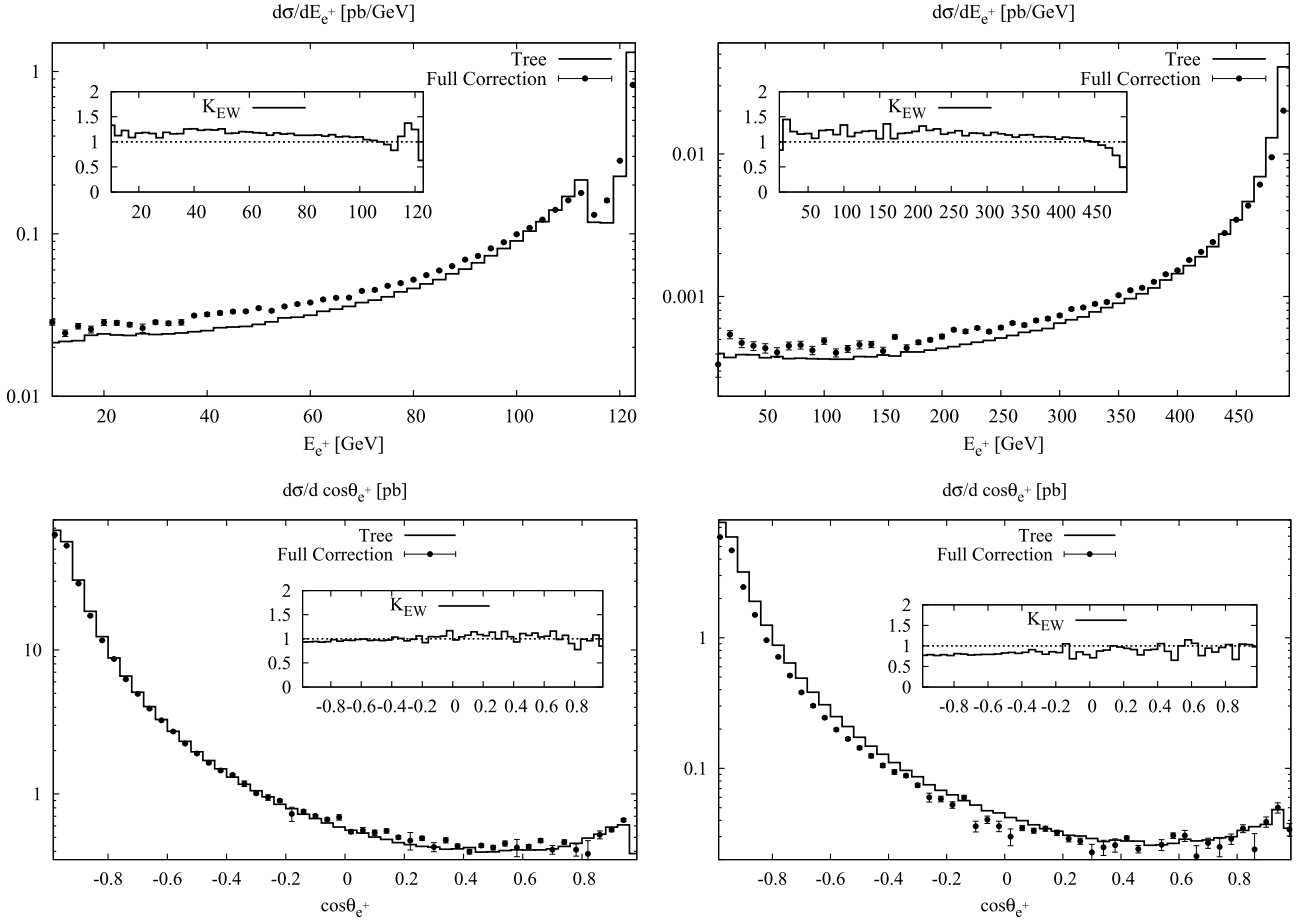


Fig. 3. Differential cross sections as a function of the positron energy and $\cos\theta_{e^+}$. In the left (right) panel $\sqrt{s} = 250$ GeV ($\sqrt{s} = 1$ TeV).

Acknowledgements

We sincerely thank Prof. F. Yuasa and Dr. N. Watanabe for their valuable discussions and comments. The authors are grateful to Prof. K. Tobimatsu and Prof. M. Igarashi for useful discussions and their contributions. The work of T.U. was supported by the DFG through SFB/TR 9 ‘‘Computational Particle Physics’’ and the work of J.V. was supported by the ERC advanced grant 320651, ‘‘HEP-GAME.’’

Appendix A

The calculation is checked numerically at a point in phase space where the four components of the particles’ momentum, $p^\mu(p_x; p_y; p_z; E)$, are

$$\begin{aligned}
 p_1^\mu & (0; 0; 499.99999999738879960679048216325; 500) \\
 p_2^\mu & (0; 0; -499.99999999738879960679048216325; 500) \\
 p_3^\mu & (-103.078628242427254979669506380205; \\
 & -114.633210803542408648432443344924; \\
 & -471.180628984259439976275161034772; \\
 & 495.759177171207049330152475391965) \\
 p_4^\mu & (8.55713405427702202967532141788216; \\
 & -14.8872000707485148244530094120855; \\
 & 72.9130813076746195344593973796190;
 \end{aligned}$$

Table 2

Test of independence of C_{UV} with respect to amplitude. For the results given in this table, the nonlinear gauge parameters are 0 and $\lambda = 10^{-21}$ GeV, and we use 1 TeV for the center-of-mass energy.

C_{UV}	$2\Re(\mathcal{M}_{Loop}\mathcal{M}_{Tree}^+)$
0	-0.142224672059345022803237910656998
10^2	-0.142224672059345022803237910656997
10^4	-0.142224672059345022803237910657050

Table 3

Test of IR finiteness of amplitude. For the results given in this table, the nonlinear gauge parameters are 0 and $C_{UV} = 0$ and the center-of-mass energy is 1 TeV.

λ [GeV]	$2\Re(\mathcal{M}_{Loop}\mathcal{M}_{Tree}^+) + \text{soft contribution}$
10^{-21}	-3.570620888259806801441498543829971 $\cdot 10^{-2}$
10^{-25}	-3.570620888259806801404094882895954 $\cdot 10^{-2}$
10^{-30}	-3.570620888259806801404090885240872 $\cdot 10^{-2}$

$$\begin{aligned}
 & 74.9077478983986818304861899869219) \\
 p_5^\mu & (94.5214941881502329499941849623225; \\
 & 129.520410874290923472885452757010; \\
 & 398.267547676584820441815763655153; \\
 & 429.333074930394268839361334621113)
 \end{aligned}$$

Tables 2–4 present the numerical results for the tests of the UV and IR finiteness and the gauge-parameter independence at this point in phase space. The results of the test of k_c -stability are presented in Table 5.

Table 4

Gauge invariance of amplitude. For the results shown in this table, we set $C_{UV} = 0$, the photon mass is 10^{-21} GeV, and the center-of-mass energy is 1 TeV.

$(\tilde{\alpha}, \tilde{\beta}, \tilde{\delta}, \tilde{\kappa}, \tilde{\epsilon})$	$2\Re(\mathcal{M}_{Loop}\mathcal{M}_{Tree}^+)$
(0, 0, 0, 0, 0)	$-0.142224672059345022803237910656998$
(10, 20, 30, 40, 50)	$-0.142224672059345022803237910657197$
(100, 200, 300, 400, 500)	$-0.142224672059345022803237910505800$

Table 5

Test of k_c -stability. The photon mass is 10^{-21} GeV and the center-of-mass energy is 1 TeV. The second column presents the soft-photon cross section and the third column presents the hard-photon cross section. The final column is the sum of both.

k_c [GeV]	σ_S [pb]	σ_H [pb]	σ_{S+H} [pb]
10^{-3}	7.873 ± 0.004	2.506 ± 0.002	10.379 ± 0.004
10^{-2}	8.401 ± 0.004	1.980 ± 0.001	10.381 ± 0.004
10^{-1}	8.932 ± 0.004	1.453 ± 0.001	10.385 ± 0.004

References

- [1] I. Božović Jelisavčić, S. Lukić, G. Milutinović Dumbelović, M. Pandurović, I. Smiljanić, JINST 8 (2013) P08012, arXiv:1304.4082 [physics.acc-ph].
- [2] K. Tobimatsu, Y. Shimizu, Prog. Theor. Phys. 74 (1985) 567–575.
- [3] K. Tobimatsu, Y. Shimizu, Prog. Theor. Phys. 75 (1986) 905–913.
- [4] M. Bohm, A. Denner, W. Hollik, R. Sommer, Phys. Lett. B 144 (1984) 414.
- [5] M. Bohm, A. Denner, W. Hollik, Nucl. Phys. B 304 (1988) 687.
- [6] F.A. Berends, R. Kleiss, W. Hollik, Nucl. Phys. B 304 (1988) 712.
- [7] J. Fleischer, J. Gluza, A. Lorca, T. Riemann, Eur. J. Phys. 48 (2006) 35, arXiv:hep-ph/0606210.
- [8] A.A. Penin, Phys. Rev. Lett. 95 (2005) 010408, arXiv:hep-ph/0501120.
- [9] A.A. Penin, Nucl. Phys. B 734 (2006) 185, arXiv:hep-ph/0508127.
- [10] R. Bonciani, A. Ferroglia, P. Mastrolia, E. Remiddi, J.J. van der Bij, Nucl. Phys. B 701 (2004) 121, arXiv:hep-ph/0405275.
- [11] R. Bonciani, A. Ferroglia, P. Mastrolia, E. Remiddi, J.J. van der Bij, Nucl. Phys. B 716 (2005) 280, arXiv:hep-ph/0411321.
- [12] R. Bonciani, A. Ferroglia, A.A. Penin, Phys. Rev. Lett. 100 (2008) 131601, arXiv:0710.4775 [hep-ph].
- [13] R. Bonciani, A. Ferroglia, A.A. Penin, J. High Energy Phys. 0802 (2008) 080, arXiv:0802.2215 [hep-ph].
- [14] S. Actis, M. Czakon, J. Gluza, T. Riemann, Phys. Rev. Lett. 100 (2008) 131602, arXiv:0711.3847 [hep-ph].
- [15] S. Actis, M. Czakon, J. Gluza, T. Riemann, Phys. Rev. D 78 (2008) 085019, arXiv:0807.4691 [hep-ph].
- [16] S. Actis, P. Mastrolia, G. Ossola, Phys. Lett. B 682 (2010) 419, arXiv:0909.1750 [hep-ph].
- [17] A.A. Penin, G. Ryan, J. High Energy Phys. 1111 (2011) 081, arXiv:1112.2171 [hep-ph].
- [18] D.Y. Bardin, W. Hollik, T. Riemann, Z. Phys. C 49 (1991) 485.
- [19] K. Tobimatsu, M. Igarashi, Comput. Phys. Commun. 136 (2001) 105.
- [20] M. Igarashi, et al., in preparation.
- [21] G. Belanger, F. Boudjema, J. Fujimoto, T. Ishikawa, T. Kaneko, K. Kato, Y. Shimizu, Phys. Rep. 430 (2006) 117, arXiv:hep-ph/0308080.
- [22] G. Belanger, F. Boudjema, J. Fujimoto, T. Ishikawa, T. Kaneko, Y. Kurihara, K. Kato, Y. Shimizu, Phys. Lett. B 576 (2003) 152, arXiv:hep-ph/0309010.
- [23] G. Belanger, F. Boudjema, J. Fujimoto, T. Ishikawa, T. Kaneko, K. Kato, Y. Shimizu, Y. Yasui, Phys. Lett. B 571 (2003) 163, arXiv:hep-ph/0307029.
- [24] G. Belanger, F. Boudjema, J. Fujimoto, T. Ishikawa, T. Kaneko, K. Kato, Y. Shimizu, Nucl. Phys. B, Proc. Suppl. 116 (2003) 353, arXiv:hep-ph/0211268.
- [25] R.-Y. Zhang, W.-G. Ma, H. Chen, Y.-B. Sun, H.-S. Hou, Phys. Lett. B 578 (2004) 349, arXiv:hep-ph/0308203.
- [26] Y. You, W.-G. Ma, H. Chen, R.-Y. Zhang, S. Yan-Bin, H.-S. Hou, Phys. Lett. B 571 (2003) 85, arXiv:hep-ph/0306036.
- [27] A. Denner, S. Dittmaier, M. Roth, M.M. Weber, Phys. Lett. B 575 (2003) 290, arXiv:hep-ph/0307193.
- [28] A. Denner, S. Dittmaier, M. Roth, M.M. Weber, Nucl. Phys. B 680 (2004) 85, arXiv:hep-ph/0309274.
- [29] A. Denner, S. Dittmaier, M. Roth, M.M. Weber, Phys. Lett. B 560 (2003) 196, arXiv:hep-ph/0301189.
- [30] A. Denner, S. Dittmaier, M. Roth, M.M. Weber, Nucl. Phys. B 660 (2003) 289, arXiv:hep-ph/0302198.
- [31] K. Kato, F. Boudjema, J. Fujimoto, T. Ishikawa, T. Kaneko, Y. Kurihara, Y. Shimizu, Y. Yasui, PoS HEP 2005 (2006) 312.
- [32] K. Aoki, Z. Hioki, R. Kawabe, M. Konuma, T. Muta, Prog. Theor. Phys. Suppl. 73 (1982) 1.
- [33] J.A.M. Vermaseren, New features of FORM, arXiv:math-ph/0010025.
- [34] J. Kuipers, T. Ueda, J.A.M. Vermaseren, J. Vollinga, Comput. Phys. Commun. 184 (5) (2013) 1453–1467.
- [35] G.J. van Oldenborgh, Comput. Phys. Commun. 58 (1991) 1.
- [36] T. Hahn, LoopTools, <http://www.feynarts.de/looptools/>.
- [37] F. Boudjema, E. Chopin, Z. Phys. C 73 (1996) 85, arXiv:hep-ph/9507396.
- [38] P.H. Khiem, J. Fujimoto, T. Ishikawa, T. Kaneko, K. Kato, Y. Kurihara, Y. Shimizu, T. Ueda, et al., Eur. Phys. J. C 73 (2013) 2400, arXiv:1211.1112 [hep-ph].
- [39] J. Fujimoto, M. Igarashi, N. Nakazawa, Y. Shimizu, K. Tobimatsu, Prog. Theor. Phys. Suppl. 100 (1990) 1.
- [40] S. Kawabata, Comput. Phys. Commun. 41 (1986) 127; S. Kawabata, Comput. Phys. Commun. 88 (1995) 309.
- [41] <http://www.mcs.anl.gov/research/projects/mpi/>.
- [42] T. Ishikawa, T. Kaneko, K. Kato, S. Kawabata, Y. Shimizu, H. Tanaka, GRACE manual, ver. 1.0, KEK Report 92-19, 1993.
- [43] Z. Hioki, Acta Phys. Pol. B 27 (1996) 2573, arXiv:hep-ph/9510269.